The Pennsylvania State University
The Graduate School
College of Earth and Mineral Sciences

CAUSES AND IMPACTS OF SEA ICE VARIABILITY IN THE SEA OF OKHOTSK USING CESM-LE

A Thesis in
Meteorology and Atmospheric Science
by
Matthew Z. Williams

Submitted in Partial Fulfillment
of the Requirements
for the Degree of

Master of Science

August 2019

The thesis of Matthew Z. Williams was reviewed and approved* by the following:

Melissa M. Gervais
Professor of Meteorology and Atmospheric Science
Thesis Advisor

Chris E. Forest
Professor of Climate Dynamics

Sukyoung Lee
Professor of Meteorology

David Stensrud
Professor of Meteorology
Head of the Department of Meteorology and Atmospheric Science

*Signatures are on file in the Graduate School.

Abstract

This study investigates the mechanisms responsible for interannual variability in sea ice coverage in the Sea of Okhotsk, located in the northwestern North Pacific, as well as the potential atmospheric response to anomalous sea ice coverage in this region. We have performed this analysis using model output from the Community Earth System Model Large Ensemble (CESM-LE). We find that thermodynamic processes involving anomalous ocean-atmosphere heat fluxes as early as late autumn affect the timing of initial sea ice growth in the Sea of Okhotsk. Low-level wind anomalies in the winter affect the extent to which sea ice fully develops, both through advection of the sea ice itself and through changes in the transport of air masses over the Sea of Okhotsk. We also find evidence that anomalous ocean-atmosphere heat fluxes in the winter trigger an atmospheric response: locally, as a negative sea-level pressure anomaly; and remotely, as a Rossby wave that extends over North America. These results are consistent with previous observational studies on interannual variability in sea ice in the Sea of Okhotsk and atmosphere-only modeling studies on the atmospheric response to changes in Sea of Okhotsk sea ice. This work provides a new perspective on the coupled processes involved in generating and responding to interannual variability of sea ice in the Sea of Okhotsk, demonstrating the ability of the CESM to capture these processes in a fully-coupled modeling framework.

Table of Contents

List of Figures

Acknowledgments

I would like to thank Dr. Melissa Gervais for her guidance throughout the entirety of this study. I am also grateful for Dr. Chris E. Forest and Dr. Sukyoung Lee for their helpful questions and insights. Thanks to the Community Earth System Model (CESM) Large Ensemble Community Project for access to CESM model output and to NSF, CISL, and Yellowstone for providing the supercomputing resources necessary for accessing that output. I am also thankful for access to ERA-Interim reanalysis products for use in this study (European Centre for Medium-range Weather Forecast (ECMWF) (2011): The ERA-Interim reanalysis dataset, Copernicus Climate Change Service (C3S) (first accessed 7-6-2018), available from https://www.ecmwf.int/en/forecasts/datasets/archive-datasets/reanalysis-datasets/era-interim). COBE SST data was provided by the NOAA/OAR/ESRL PSD, Boulder, Colorado, USA, from their Web site at https://www.esrl.noaa.gov/psd/. Lastly, I would like to thank the Pennsylvania State University Department of Meteorology and Atmospheric Science for providing my funding throughout my time in this program.

Chapter 1 Introduction

1.1 Importance of Sea Ice - Atmosphere Research

As a result of anthropogenic climate change, sea ice in the northern hemisphere is experiencing an overall decline – becoming increasingly thinner and covering a smaller spatial extent. Simulations by the Community Earth System Model (CESM) project the central Arctic to become seasonally ice-free within the next few decades (Jahn et al., 2016). A variety of economic and geopolitical implications will result, such as the opening of trans-Arctic shipping routes (Gascard et al., 2017; Melia et al., 2017). Predicting interannual variability of Arctic sea ice will be important for determining whether shipping routes will be clear of sea ice and safe to pass. There is also considerable interest in how changes in Arctic sea ice might influence atmospheric circulation in the mid-latitudes. If sea ice variability has a significant impact on atmospheric circulation, this could also be a source of predictability for atmospheric variability.

The Sea of Okhotsk (hereafter, SOK; Fig. 1.1), located south of the Arctic Circle, north of the Kuril Islands and west of the Kamchatka Peninsula, is *already* seasonally ice-free and has large interannual variability in its wintertime sea ice coverage. Thus, sea ice in this region provides a useful test case for understanding the dominant processes involved in producing interannual variability in seasonal ice cover, although we do expect different Arctic regions to have some different sources of variability. Furthermore, within the SOK, it is possible to assess the ability of an Earth system model to represent the causes and impacts of this variability through comparison with observations. Previous studies have documented some factors likely responsible for this interannual sea ice variability within the SOK (e.g., Ohshima et al., 2006; Sasaki et al., 2007) and some atmospheric conditions that may arise due to this interannual variability (e.g., Honda et al., 1999; Screen, 2017).

Figure 1.1: The Sea of Okhotsk, extending roughly from 45°N to 60°N and from 140°E to 155°E.

1.2 Literature Review of Sea of Okhotsk Research

1.2.1 Conditions Leading to Anomalous Wintertime SOK Sea Ice Coverage

Through patterns of atmospheric variability, mechanisms occurring on the timescale of multiple seasons (Ogi et al., 2015) and even multiple years (Ukita et al., 2007) have been proposed to explain SOK sea ice variability. During the Northern Hemisphere winter period from 1979-2013, the leading mode of sea ice variability is a "double seesaw" pattern – with positive anomalies in the Greenland Sea, the Barents Sea, and the SOK and with negative anomalies in the Bering and Labrador Seas (Close et al., 2017). This pattern has been attributed to the North Atlantic Oscillation (NAO) (Ukita et al., 2007), while a similar pattern of sea ice variability focused on the North Pacific marginal sea ice zones has been attributed in part to the Arctic Oscillation (AO) (Liu et al., 2007). For the AO, anomalous low-level flow integrated over the course of the year may result in low-level temperature anomalies that lead to altered sea surface temperatures (SSTs) in the SOK (Ogi et al., 2015). The proposed relationship of the NAO and SOK sea ice variability is more complex, involving interactions with various marginal sea ice zones around the Arctic (Ukita et al., 2007).

In addition to these large-scale modes of variability, local thermodynamic and dynamic processes have been shown to play an important role in SOK variability in observations. Through analyzing observations, Ohshima et al. (2006) found that October-November surface heat flux from the sea to the atmosphere in the northwestern SOK is negatively correlated with 10-day averaged sea ice coverage through mid-January. Nakanowatari et al. (2010) showed that 850 mb temperature anomalies in the vicinity of the SOK, as well as SST anomalies in the western Bering Sea, in late autumn and early winter have a significant negative relationship with maximum SOK sea ice coverage. These studies demonstrate how preconditioning of SSTs either due to anomalously positive (negative) autumn heat fluxes from the sea to the atmosphere or advection of anomalously cold (warm) SSTs can increase (inhibit) the formation of sea ice in the winter.

In the winter months, atmospheric dynamical processes also become important for determining the coverage of sea ice in the SOK. Anomalous gradients in sea-level pressure between the Aleutian low and Siberian high are an important factor for the interannual sea ice variability in the SOK (Close et al., 2017; Parkinson, 1990). This sea-level pressure gradient dictates the low-level wind direction and the type of air mass present over the SOK, both of which likely modulate the ultimate extent of sea ice coverage (Sasaki et al., 2007). Namely, low-level winds that act to transport sea ice away from the coast lead to enhanced ice growth. A colder, continental air mass transported over the SOK region by those low-level winds results in a larger temperature difference between the sea and atmosphere, leading to an enhanced local cooling of SSTs and increased sea ice formation. The inverse is true for low-level winds that oppose the transport of sea ice away from the coast, the result being reduced ice growth.

1.2.2 Atmospheric Response

Sea ice in the SOK has been shown to impact atmospheric circulation both in observational analyses (Alexander et al., 2004; Honda et al., 1999; Mesquita et al., 2011) and modeling experiments with anomalous SOK sea ice (Honda et al., 1999; Mesquita et al., 2011; Screen, 2017; Sun et al., 2015). A primary feature of the response is a stationary Rossby wave that extends from the SOK over North America (Alexander et al., 2004; Honda et al., 1999; Screen, 2017; Sun et al., 2015). February is the month when the product of total surface heat flux and SIE anomalies is maximized (Screen, 2017), and therefore, it is the month with the greatest potential for anomalous SOK sea ice coverage to force an atmospheric response. Associated with this potential Rossby wave response, sea ice variability in the SOK affects storm track activity in the North Atlantic through cyclone seeding (Mesquita et al., 2011); i.e., transient upper-level troughs formed over the North Pacific in response to SOK sea ice anomalies can eventually lead to enhanced extratropical cyclone formation in the North Atlantic.

Other studies have shown effects of the vertical propagation of disturbances in response to anomalous SOK sea ice coverage. Peings and Magnusdottir (2013) concluded that weakening of stratospheric westerlies in proximity to the SOK resulted from constructive interference of the climatological stationary wave over the North Pacific basin with the Rossby wavetrain generated in response to increased surface heat flux over the SOK. However, Screen (2017) suggested that stratospheric polar vortex weakening is driven primarily through anomalously low sea ice coverage in the Barents-Kara Sea rather than in the SOK. Sun et al. (2015) provided evidence, based on anomalously low sea ice coverage over the SOK and Bering Sea, that the resultant Rossby wavetrain actually interferes *destructively* with the climatological stationary wave, thus enhancing the stratospheric polar vortex.

1.3 Research Purpose

Previous studies were limited by focusing on specific processes that facilitated anomalous sea ice coverage, such as the thermodynamic staging in autumn (Ohshima et al., 2006; Sasaki et al., 2007) or the dynamic forcing in winter (Close et al., 2017), or by only focusing on the influence of atmospheric conditions by the anomalous sea ice coverage (Honda et al., 1999; Mesquita et al., 2011; Screen, 2017). Also, each of the mechanisms for forcing SOK interannual variability has only been analyzed using observational data. In this study, we use the CESM, a fully-coupled Earth system model, to examine the progression of conditions preceding and following anomalous February sea ice coverage in the SOK. Given the limitations of previous work, we seek to answer three questions:

1. What mechanisms are responsible for anomalous sea ice extent in the SOK?
2. How does the atmosphere respond to anomalous SOK sea ice extent?
3. Can the CESM represent these processes, which have been documented in observational analyses and idealized modeling experiments?

The data and methods that were chosen to answer these questions are documented in Chapter 2. The conditions preceding and following anomalous February SOK sea ice coverage are presented in Chapter 3. Lastly, Chapter 4 contains a summary of the main findings and mentions potential future research directions following this study.

Chapter 2 Data and Methods

2.1 Data

2.1.1 Model

To identify atmospheric and oceanic conditions associated with anomalous wintertime sea ice coverage in the SOK, we analyzed the model outputs from the CESM Large Ensemble project (CESM-LE) (Kay et al., 2015). CESM-LE is an ensemble of 40 simulations using an Earth system model that has fully coupled components representing the atmosphere, ocean, land, and sea ice systems. Of these 40 members, we selected 30 for use in this study. The only discrepancies between members are perturbations in the initial air temperature field on the order of 10^{-14} K. Therefore, the non-linear effects of chaotic internal variability in Earth's climate system generate the differences from member to member (Kay et al., 2015), and averaging over multiple members can help to eliminate the effects of this variability and to enhance signal-to-noise ratio.

Each member of CESM-LE employs approximately 1°x1° horizontal resolution for all of its components. The atmospheric component, Community Atmosphere Model version 5 (CAM5) (Hurrell et al., 2013), has 30 vertical levels; the oceanic component, Parallel Ocean Program version 2 (POP2) (Smith et al., 2010), has 60 vertical levels. The last two components are the Community Land Model version 4 (CLM4) (Lawrence et al., 2011; Oleson et al., 2010) and the Community Ice CodE version 4 (CICE4) (Hunke and Lipscomb, 2008). The CICE4 component represents sea ice with five thickness categories (Rothrock, 1975; Thorndike et al., 1975), uses an energy-conserving thermodynamic scheme (Bitz and Lipscomb, 1999), and includes boundary conditions forced by both atmospheric and oceanic stresses (Hunke and Dukowicz, 2002). A known positive northern hemisphere annual-mean sea ice bias exists when CICE4 is coupled within CESM, corresponding to an underprediction of the global mean temperature trend of recent decades as is common among most Coupled Model Intercomparison Project Phase 5 (CMIP5) models (Rosenblum and Eisenman, 2017).

There are three main advantages of using CESM-LE for this study. First, as a fully-coupled Earth system model, CESM outputs are generated by the fully-coupled processes between the atmosphere, sea, and sea ice that may influence SOK sea ice coverage. A limitation of using CESM for this purpose is that causality of conditions in one or more component forcing responses in another is not able to be proven, unlike targeted experiments in which responses within a single-component general circulation model are forced by prescribing a certain condition. Second, CESM-LE provides a larger sample size of winters having anomalous sea ice coverage in the SOK, which leads to higher statistical significance. Third, by having a large sample size, this shortens the required time increments for analyzing the progression of conditions preceding and following winters of anomalous sea ice. Most previous studies employ seasonal or monthly averages in order to smooth out synoptic-scale variability; with the large sample size that CESM-LE provides, that variability is effectively reduced, even when only considering weekly averages.

2.1.2 Observations

For comparison with the modeled connection of atmospheric and oceanic conditions with SOK sea ice variability, we used multiple observation-based products for the atmosphere, ocean, and sea ice. The ERA-interim reanalysis product (Dee et al., 2011) provides atmospheric information with horizontal resolution of approximately 80km x 80km on 60 vertical levels. COBE SST data (Ishii et al., 2005) contains monthly-averaged SST data on a 1° latitude x 1° longitude grid. The sea ice product, NOAA/NSIDC Climate Data Record of Passive Microwave Sea Ice (Meier et al., 2017; Peng et al., 2013), implements a combination of two algorithms to yield more accurate SIC estimates from satellite data retrieval. These SIC estimates have a horizontal resolution of 25km x 25km.

2.2 Methods

We analyzed SOK sea ice coverage and atmospheric variables for the years of 1980-2000. We chose this time period because the CESM-LE ensemble-averaged sea ice extent (SIE) showed no significant trend (Fig. 2.1) and because observational data products were available for these years. For this study, we defined SIE as the total area of grid boxes having at least 15 percent sea ice concentration (SIC), where SIC is the fraction of a grid box covered by sea ice.

The CESM-LE has both a large sample size and a wide range of variability in SIE over the analysis period, which is ideal for identifying a coherent signal in conditions associated with extreme SIE. Within the model analysis, we defined the thresholds for extreme cases as the tenth and ninetieth percentiles of SIE values in February for all ensemble-year combinations (e.g., ensemble member 3 in

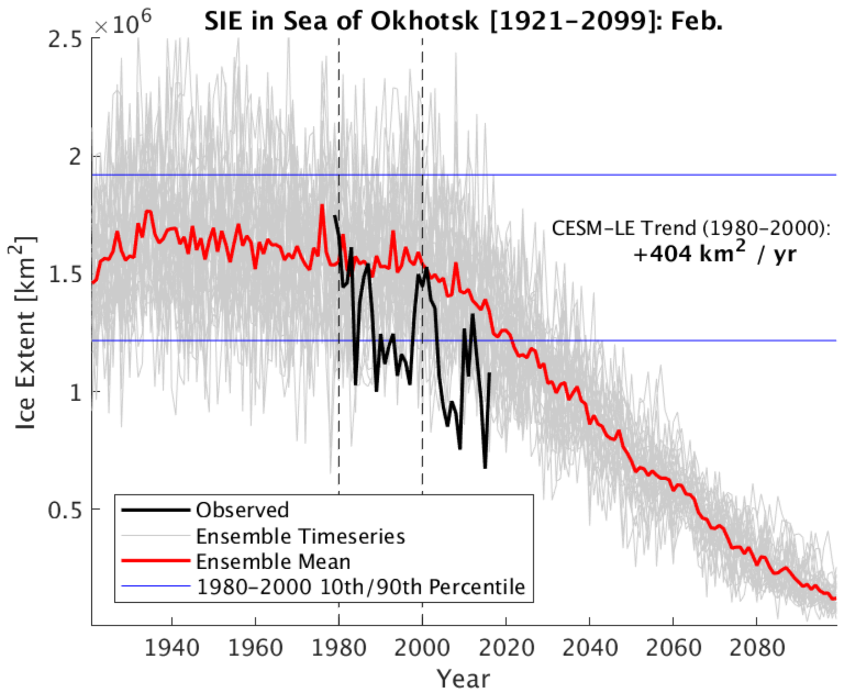

Figure 2.1: CESM-LE representation of February total SIE in the SOK from 1921-2099. The dashed vertical lines show the years of this study, 1980-2000. Points in between these dashed lines and above the top blue line (below the bottom blue line) comprise the High (Low) regime cases. Observed SIE from 1979-2016 is shown in the solid black line.

1986). We classified individual ensemble-year combinations with SIE values less (greater) than the 10^{th} (90^{th}) percentile as belonging to the Low (High) sea ice regime (Fig. 2.1).

For the observations, we chose the five years of least (greatest) February-averaged SIE to comprise the Low (High) regime. Those years, ordered from most-extreme to least-extreme, were 1989, 1984, 1997, 1994, and 1991 (1980, 1983, 1987, 1999, and 1986). These instances of observed extreme February SIE in the SOK lie outside of roughly the 25^{th} and 75^{th} percentiles, whereas the instances of modeled extreme SIE lie outside of the 10^{th} and 90^{th} percentiles. This reduced magnitude in variability will likely result in smaller atmospheric forcing and response associated with the high and low SIE in the observations.

Seasonal cycles for both the model and the observations are shown in Figure 2.2, including the mean, 10^{th} to 90^{th} percentiles, and composites of the High and Low SIE regimes. In comparing the modeled and observed SIE seasonal cycle, there is a notable bias in the model SIE in both the timing of the seasonal sea ice cycle and the maximum SIE value. In the model, the SOK is typically ice-free from July to November and the average SOK SIE reaches a maximum in March of approximately

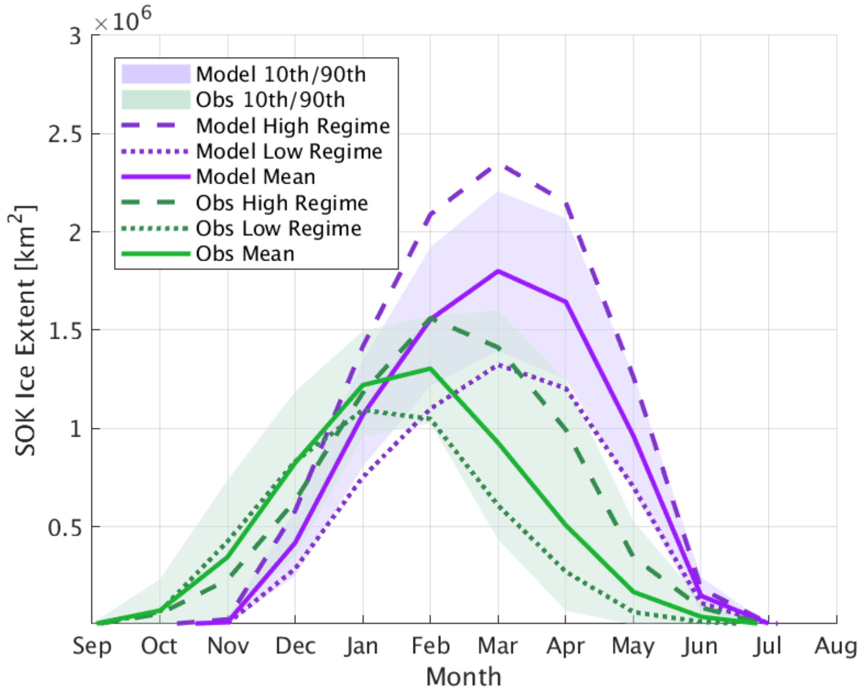

Figure 2.2: Annual cycle of SIE in the SOK. CESM-LE (observed) SIE curves are purple (green). The shaded regions are bounded by the 10^{th} and 90^{th} percentiles for each month. The solid curves depict the monthly means for the modeled and observed SIE. The dashed (dotted) curves depict the composite-mean SIE for the High (Low) regime.

1.75×10^6 km^2. SOK sea ice in the observations begins to grow in September and reaches a mean maximum in February at a smaller value of approximately 1.25×10^6 km^2.

In addition to the mean biases between the model and the observations, there are also differences in the shape of the seasonal cycles of the High and Low regimes. In the model, High and Low regime curves remain near the 90^{th} and 10^{th} percentile values for each month from December to May, indicating a large autocorrelation of SOK sea ice within CESM-LE. Unlike the model, the observed Low regime SIE closely follows the mean SIE until January, after which we see lower values of SIE throughout the rest of the ice covered season. The High regime has lower SIE than average through the months of October to December, after which there is a marked increase in SIE until February (Fig. 2.2). The observations consist of only 5 members, each of whom have large differences in their seasonal cycles that impact the ensemble mean (not shown). It is difficult to assess whether the seasonal cycle differences between the observations and the model in both regimes are the result of these sampling limitations or of differences in mechanisms.

To investigate the atmospheric and oceanic conditions associated with anomalous SIE for the Low and High sea ice regimes, we evaluated composite anomalies of turbulent heat flux (THF), mean sea-level pressure (SLP), 850 hPa potential temperature (θ_{850}), 500 hPa geopotential height (Z_{500}), 850 hPa wind (U_{850}), near-surface wind (U_{BOT}), and sea surface temperature (SST). THF is the sum of sensible and latent heat flux. At each grid point, for a given time period (e.g., February), we calculated composite anomalies by first subtracting the average value for all years from each of the values in the High/Low regime, and then averaging all of those differences.

Previous studies involving atmosphere and SOK sea ice relations have analyzed monthly-averaged (Screen, 2017; Yamamoto et al., 2006) or seasonally-averaged (Alexander et al., 2004; Close et al., 2017; Honda et al., 1999; Sasaki et al., 2007) fields. However, atmospheric forcing of and response to anomalous sea ice coverage can occur on timescales of a few days (Fang and Wallace, 1994). To gain more insight into these processes that have shorter timescales, in the present study, we analyzed a progression of weekly-averaged, modeled composite fields. We first, however, included the monthly-averaged fields for August through November, so as to analyze potentially important features such as persistent SST anomalies or atmospheric waves. We then began the weekly-averaged portion, which spanned twenty weeks from the week beginning on November 23 to the week ending on April 11, for each of the regimes. Statistical significance was evaluated for the modeled composite anomalies using the two-sided Student's t-test.

Additionally, monthly-averaged, observed composite fields were analyzed from August of the year prior to anomalous sea ice coverage to March of the year after. Weekly composites were not analyzed in the observations due to the small sample size. Furthermore, due to small sample size, significance was almost nonexistent for the observed composite anomalies at the five percent level and was therefore not shown in the results.

For brevity, only the results from the Low regime will be shown in the next section. We conjecture that the same mechanisms are responsible for both anomalously high and low wintertime SOK sea ice coverage, and it is these mechanisms that we are interested in understanding further. Results from the High regime are generally similar but of opposite sign to those from the Low regime. High regime results are shown in Appendix A.

Chapter 3
Results

3.1 Processes Leading to Anomalous Wintertime SOK Sea Ice Coverage

3.1.1 Multi-seasonal SST Anomaly Presence

The earliest signs of conditions preceding anomalous sea ice coverage occur in the SST field and are identified in the modeled progression of monthly-averaged SST composite anomalies in and around the SOK (Figs. 3.1 and 3.2). Positive SST anomalies tend to exist in the winter one year prior to anomalously low sea ice along the Kamchatka Peninsula coast and into the western Bering Sea in the model (Fig. 3.1). SST anomalies also appear over the eastern SOK in the spring prior in the observations (Fig. 3.2). These results are consistent with Deser et al. (2003), who showed that SSTs in this region have a fairly high interannual autocorrelation. The magnitudes of the SST composite anomalies are highest in February and March at the peak of the sea ice anomalies and have a secondary peak in the late summer months in the model composites (Fig. 3.1). This late summer peak is even more pronounced in observations, where the anomalies are even greater than those in February and March (Fig. 3.2). Previous work by Ogi et al. (2015) demonstrated a negative relationship between the annual AO index and SSTs across the central and southeastern SOK in these summer months. This relationship may indicate an indirect link between the annually-integrated AO and anomalous February SOK sea ice coverage.

3.1.2 Autumn Thermodynamic Preconditioning

As mentioned previously, multiple studies have demonstrated the importance of thermodynamic conditions in setting the stage for anomalous wintertime sea ice coverage in the SOK. Consistent with Ohshima et al. (2006), negative turbulent heat flux (THF) anomalies appear over the northwestern

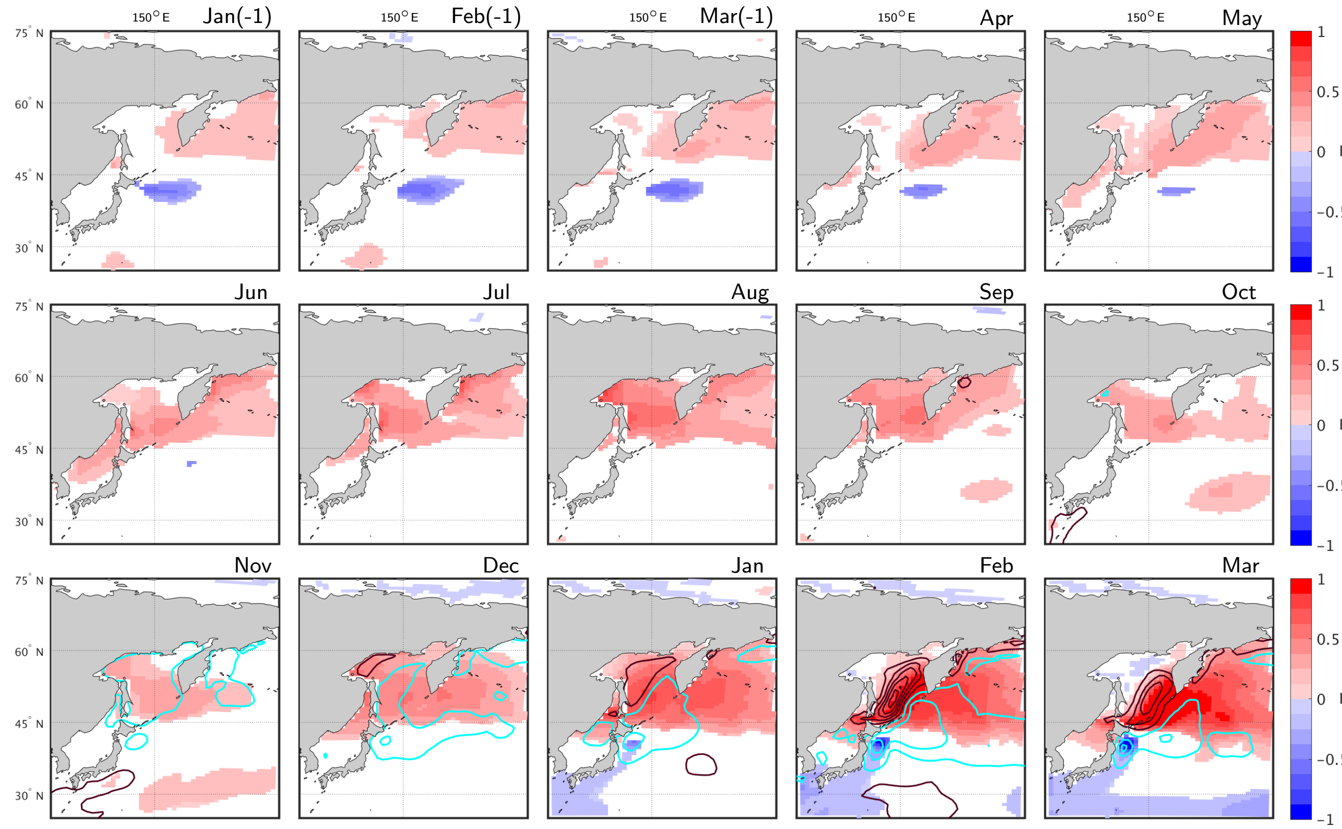

Figure 3.1: Modeled monthly SST anomalies (shaded) and THF anomalies (contours) for the Low regime. Top row contains monthly-averaged values, while other rows contain weekly-averaged values. Contours begin at +/- 10 Wm^{-2} and have an interval of 20 Wm^{-2}. Positive (negative) THF anomalies are shown by maroon (cyan) contours and correspond to heat transfer out of (into) the surface. Only SST anomalies that are statistically significant at the α=0.05 level are shown.

SOK in October, growing in magnitude and spreading over the remaining portions of the sea into December (Figs. 3.1 and 3.2). These negative THF anomalies indicate a reduction of late autumn oceanic heat loss to the atmosphere compared to average. The opposite effect occurs prior to anomalously high sea ice coverage, with an abundance of late autumn oceanic heat loss (Appendix A).

THF is modulated by multiple factors, including temperature contrast between the sea surface and low-level atmosphere, as well as low-level atmospheric relative humidity and wind speed. In November, the aforementioned temperature contrast is altered, with SST and θ_{850} anomalies both present for the SOK (Figs. 3.1 and 3.2; Figs. 3.5 and 3.6). Wind speed is also reduced at this time, as easterly wind anomalies oppose the westerly mean wind (Figs. 3.3 and 3.4; mean wind not shown). This implies that both anomalous air-sea temperature contrast and decreased wind speed in autumn contribute to the THF anomalies in the SOK.

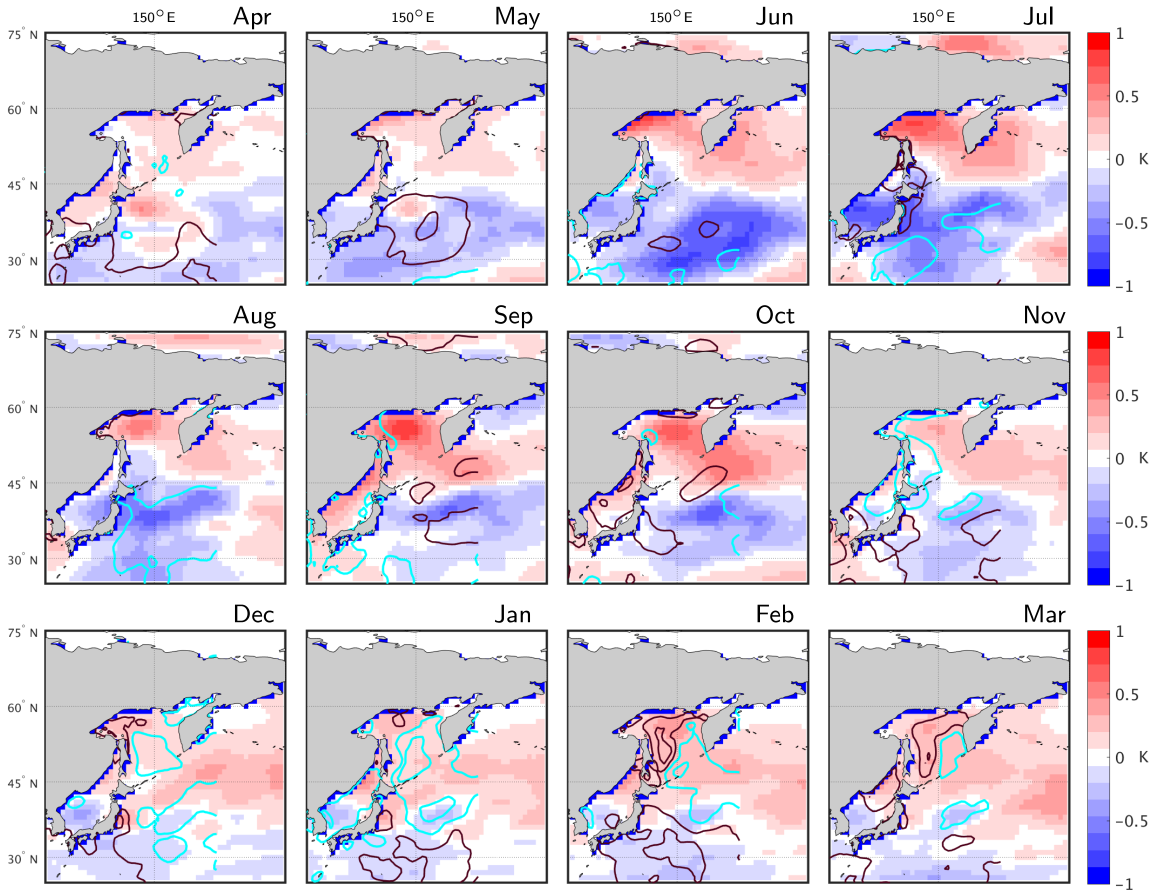

Figure 3.2: Observed monthly SST anomalies (shaded) and THF anomalies (contours) for the Low regime. Contours begin at +/- 10 Wm^{-2} and have an interval of 20 Wm^{-2}. Positive (negative) THF anomalies are shown by maroon (cyan) contours and correspond to heat transfer out of (into) the surface. Statistical significance not shown.

The θ_{850} anomalies in the autumn prior to abnormal SOK February sea ice coverage may result from anomalous temperature advection (Figs. 3.5 and 3.6). Low-level winds in the region surrounding the SOK are modulated through the relative strengths and locations of both the Aleutian low and Siberian high. Two discrete stationary Rossby waves, one originating from the eastern North Atlantic into north-central Asia and the other from the western North Pacific into western Canada, influence the relative strengths and locations of those two systems in the autumn months (Sasaki et al., 2007). Both the modeled and observed October and November Z_{500} composite anomalies do show some semblance of a Rossby wave structure (Figs. 3.7 and 3.8), although the locations of the centers of action are somewhat different compared to Sasaki et al. (2007). This particular circulation structure favors anomalous low-level flow over the SOK from the central North Pacific, establishing a milder, maritime air mass that tends to persist for multiple weeks (Figs. 3.5 and 3.6). Therefore, this stationary Rossby wave present during October and November may produce conditions that are conducive to altering the exchange of heat between the sea surface and the atmosphere, thereby changing the timing of initial sea ice formation in the SOK.

3.1.3 Winter Forcing

Once sea ice has developed, dynamic factors such as the direction of low-level winds also become important for determining to what extent sea ice will grow in the SOK. For the Low regime, low-level wind anomalies throughout the winter in the model, and in January in the observations, are primarily from the east-southeast over the southeastern half of the SOK (Figs. 3.3 and 3.4). These wind anomalies are present in conjunction with a noticeably weaker Aleutian low, as demonstrated by the anticyclonic SLP anomalies over the North Pacific (Figs. 3.7 and 3.8). These anomalous low-level winds allow for a more prevalent, maritime air mass over the SOK (Figs. 3.5 and 3.6), which may prevent sea surface cooling over the southeastern SOK necessary for new sea ice growth in the winter months.

In addition to those thermodynamic effects, these anomalous low-level winds can mechanically inhibit the expansion of preexisting sea ice into the southeastern SOK. This effect can be seen clearly throughout December into mid-February, as the wind anomalies are oriented in a nearly perpendicular manner to the sea ice edge, opposing the direction of sea ice expansion (Fig. 3.3). This same effect is observed in January (Fig. 3.4), although the sea ice edge is less well-defined. A similar but opposite mechanism occurs during the High regime, with wind anomalies aiding the sea ice expansion, which promotes additional sea ice growth in this season (Appendix A).

3.2 Atmospheric Response to Anomalous Wintertime SOK Sea Ice Forcing

3.2.1 Near-field Response

Previous studies have shown that THF anomalies produced due to anomalous sea ice coverage can provide forcing for an atmospheric response (e.g., Screen, 2017). From December to February, THF anomalies over the central SOK transition from negative to positive, coincident with the advancement of the sea ice edge (Figs. 3.3 and 3.4). In February of the Low regime composites, positive THF anomalies exceeding 100 $\mathrm{Wm^{-2}}$ exist in both the weekly- (Fig. 3.3) and monthly-averaged (Fig. 3.1) composites in the central SOK in the model. For the observations, these positive THF anomalies are located further west and exceed 30 Wm^{-2} in February (Fig. 3.2). We expect the magnitude of the THF in the observations to be lower than in the model because the composites consists of only 5 events out of 21 years and so the threshold is closer to the 25^{th} percentile rather than the 10^{th} used for the model. The discrepancy in the location can be explained by the CESM-LE positive sea ice bias, which causes the variable sea ice edge to be located further east.

Where the sea ice edge does not reach the climatological wintertime location, a much stronger temperature contrast exists between the surface and the air above. This enhanced temperature contrast leads to a large transfer of heat from the sea surface into the atmosphere, which would contribute to the low-level temperature anomalies. There is a localized positive θ_{850} anomaly to the southeast of the SOK during the weeks of 2/15 through 3/14 (Fig. 3.5) consistent with the atmospheric response to a such a turbulent heat flux anomalies. However, this cannot be separated from the forcing mechanism for low sea ice discussed above. This feature also appears in the observed θ_{850} anomaly field during February (Fig. 3.6).

In both the model and the observations, the positive SLP anomaly over the SOK is reduced and a negative SLP anomaly also develops to the south of the SOK (Figs. 3.7 [2/15 - 2/21 and 3/8 - 3/14] and 3.8 [Feb.]). Around the same time, we see a shift of anomalous near-surface wind direction (Figs. 3.3 [from 2/1 - 2/7 to 3/1 - 3/7] and 3.4 [from Jan. to Feb.]). The wind shift is especially pronounced in the model, reversing from east-southeasterly to northwesterly over the south-central SOK.

The theoretical local atmospheric linear response to a shallow thermal forcing in a steady background flow is baroclinic with the formation of a surface low located a quarter-wavelength downstream, along with a peak in low-level temperature. This theory also suggests that low-level winds with an equatorward component should develop, as cold air advection typically balances the thermal forcing in the mid-latitudes (Hoskins and Karoly, 1981; Vallis, 2017). Therefore, this combination of a negative SLP anomaly, localized positive θ_{850} anomaly, and near-surface wind shift is a plausible atmospheric response to the anomalously low sea ice coverage, although in this case the background flow is not in steady state.

3.2.2 Far-field Response

In addition to local atmospheric conditions, some non-local modeled and observed conditions are consistent with both the theoretical response to shallow mid-latitude heating and the demonstrated atmospheric response to low sea ice coverage in the SOK from previous studies. Further downstream of the heat source from the warm surface low, an upper-level high is expected to form (Hoskins and

Karoly, 1981; Vallis, 2017). We notice the eastward shift of the center of positive Z_{500} anomalies in the model (Fig. 3.7 [from 2/8 - 2/14 to 3/1 - 3/7]), which seems to be consistent with this theory. Similarly, the observed positive Z_{500} anomalies in January occur broadly across the North Pacific and become more constrained to the eastern North Pacific in February. While not as apparent as the signal from the model, this observed transition of positive Z_{500} anomalies could be related to the theoretical non-local atmospheric response to anomalous heating associated with the low sea ice coverage.

The pattern of Z_{500} anomalies in the model, especially during the week of 3/8 - 3/14, and that in the March observations, resembles the Rossby wave patterns shown in Honda et al. (1999) and Screen (2017). These studies utilized atmospheric models forced with prescribed sea ice and SSTs and so were able to directly attribute their atmospheric responses to changes in SOK sea ice. The similarity of this Rossby wave pattern to those in Honda et al. (1999) and Screen (2017) therefore suggests that the ensuing Rossby wave in this study is indeed a response to the anomalous sea ice conditions in SOK.

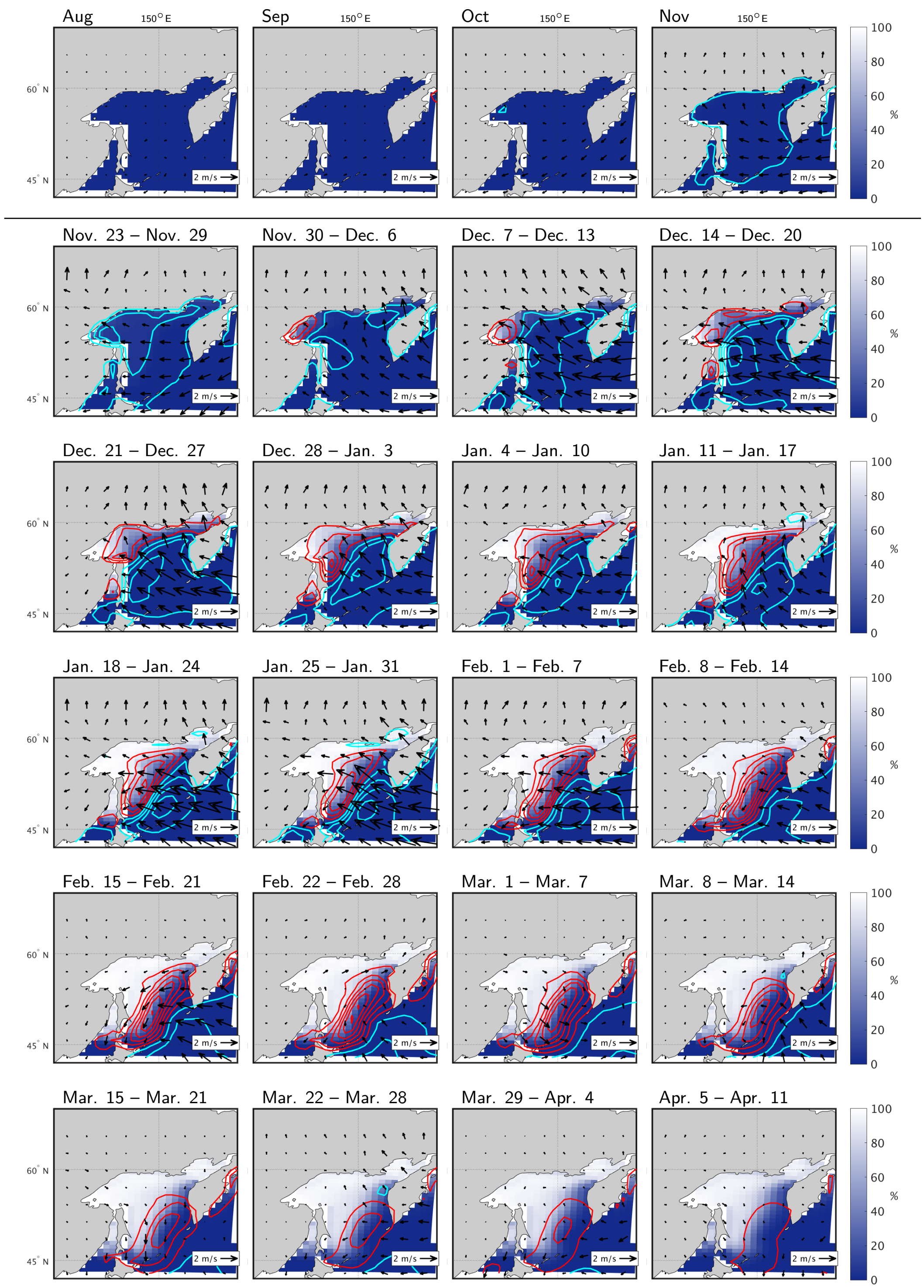

Figure 3.3: Modeled total sea ice concentration (shaded) with THF anomalies (contours) and near-surface wind anomalies (arrows) for the Low regime. Top row contains monthly-averaged values, while other rows contain weekly-averaged values. Contours begin at +/- 10 Wm^{-2} and have an interval of 20 Wm^{-2}. Positive (negative) THF anomalies are shown by red (cyan) contours.

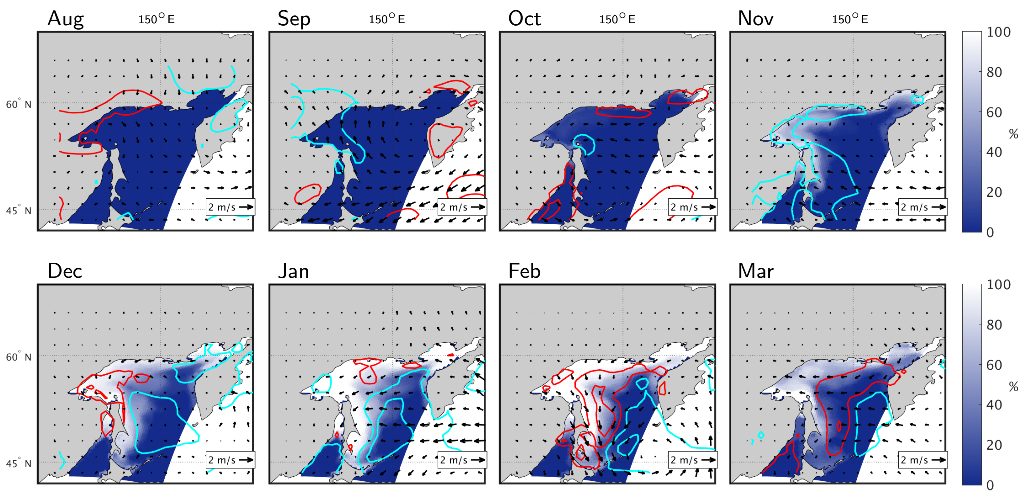

Figure 3.4: Observed monthly total sea ice concentration (shaded) with turbulent heat flux anomalies (contours) and near-surface wind anomalies (arrows) for the Low regime. Contours begin at +/- 10 Wm^{-2} and have an interval of 20 Wm^{-2}. Positive (negative) THF anomalies are shown by red (cyan) contours.

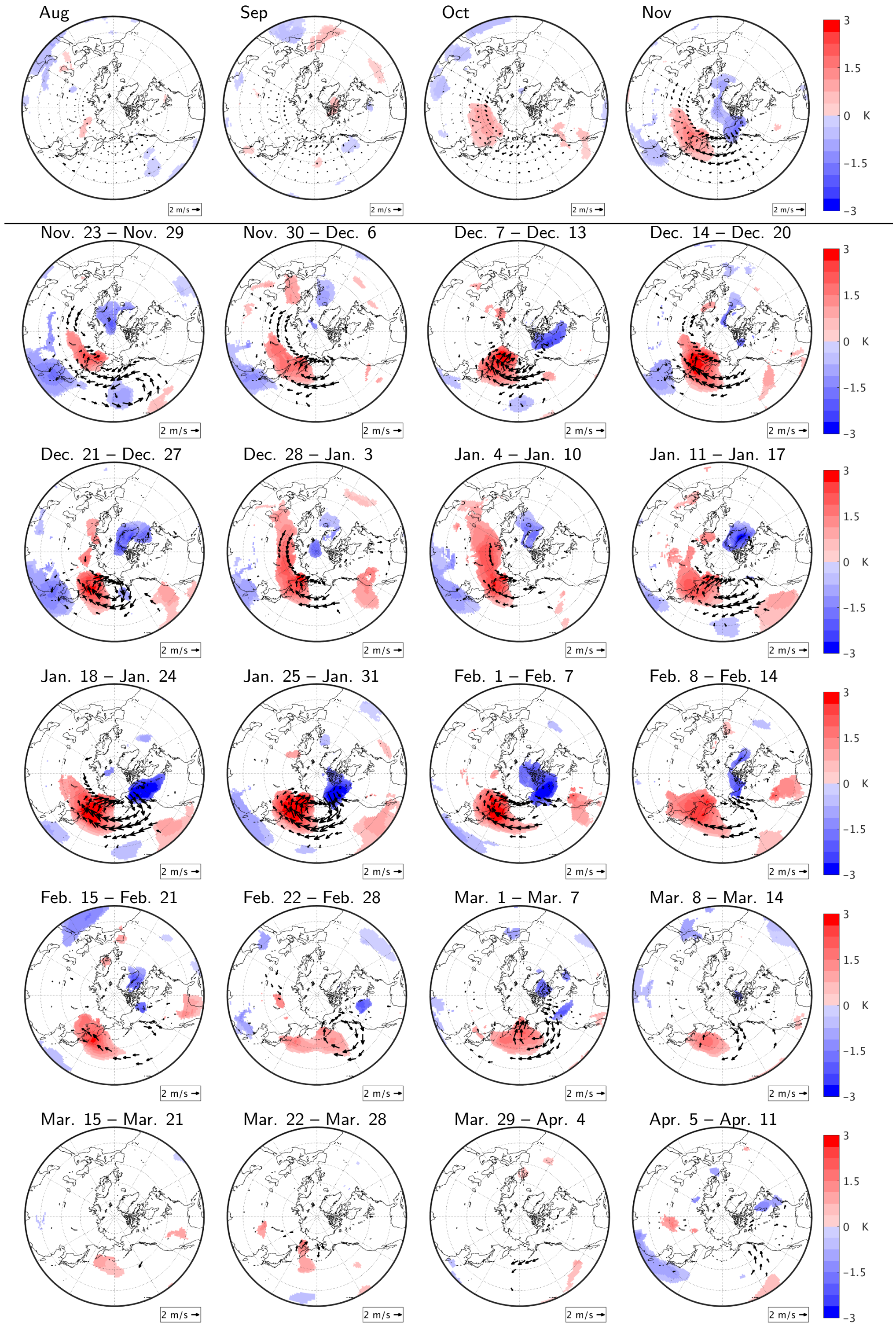

Figure 3.5: Modeled 850 mb atmospheric anomalies: θ_{850} anomalies (shaded) and wind anomalies (arrows) for the Low regime. Top row contains monthly-averaged values, while other rows contain weekly-averaged values. Plotted anomalies are statistically significant at the α=0.05 level.

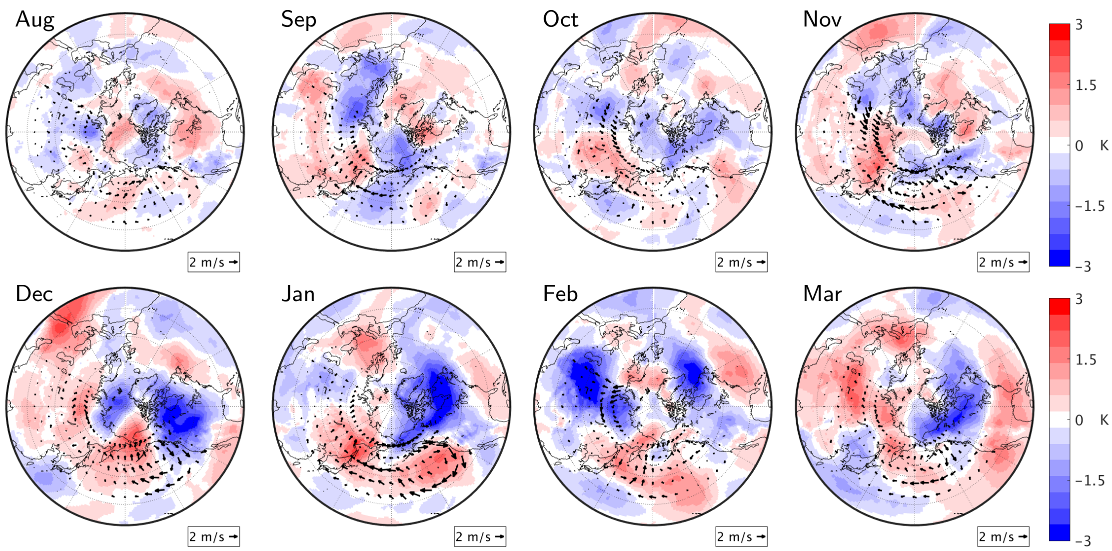

Figure 3.6: Observed monthly 850 mb atmospheric anomalies: θ_{850} anomalies (shaded) and wind anomalies (arrows) for the Low regime. Statistical significance not shown.

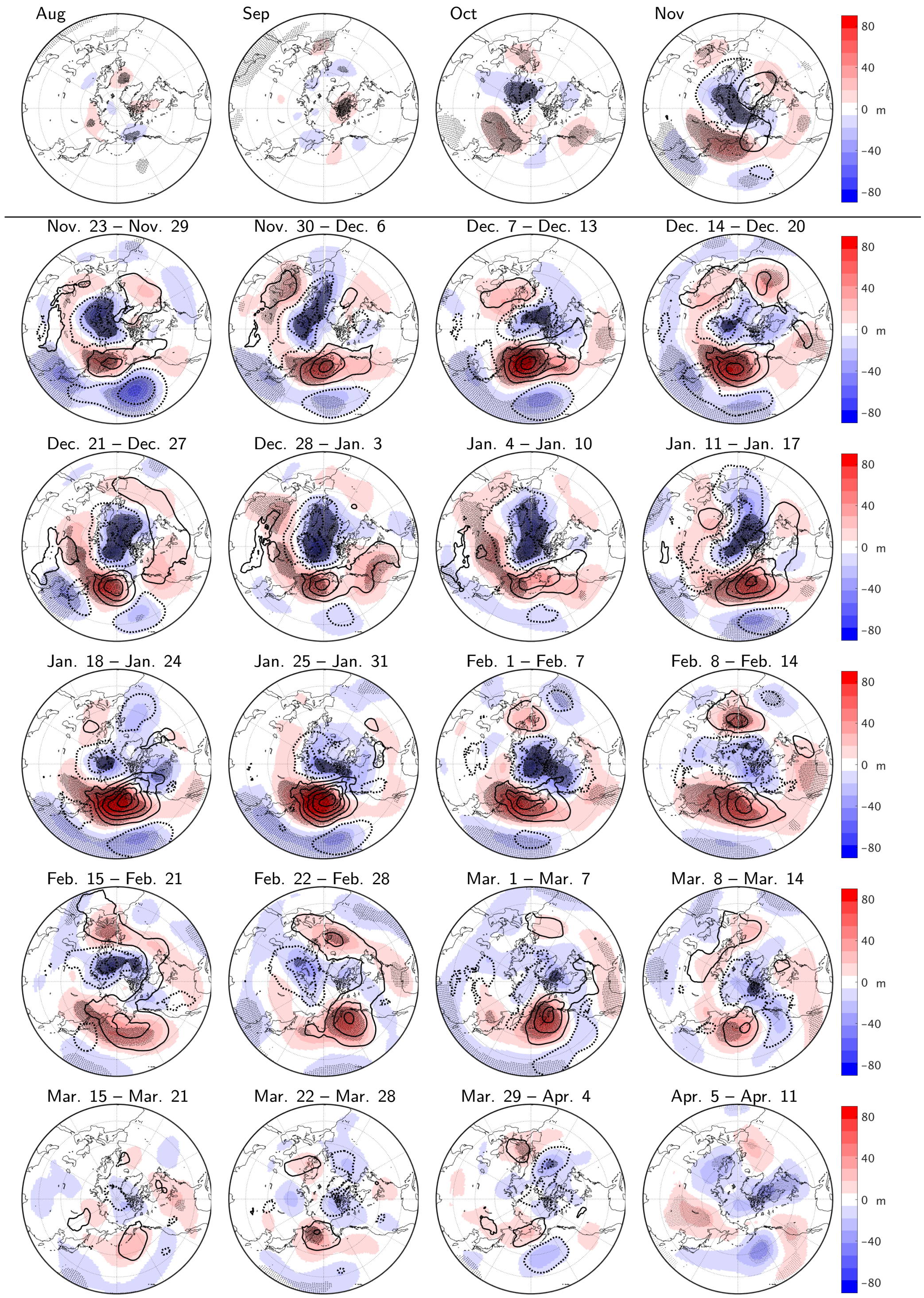

Figure 3.7: Modeled 500 mb geopotential height anomalies (shaded) and sea- level pressure anomalies (contours) for the Low regime. Top row contains monthly-averaged values, while other rows contain weekly-averaged values. Contours begin at +/- 1 mb and have an interval of 2 mb. Positive (negative) SLP anomalies are shown by solid (dotted) contours. Geopotential height anomalies are stippled if statistically significant at the α=0.05 level.

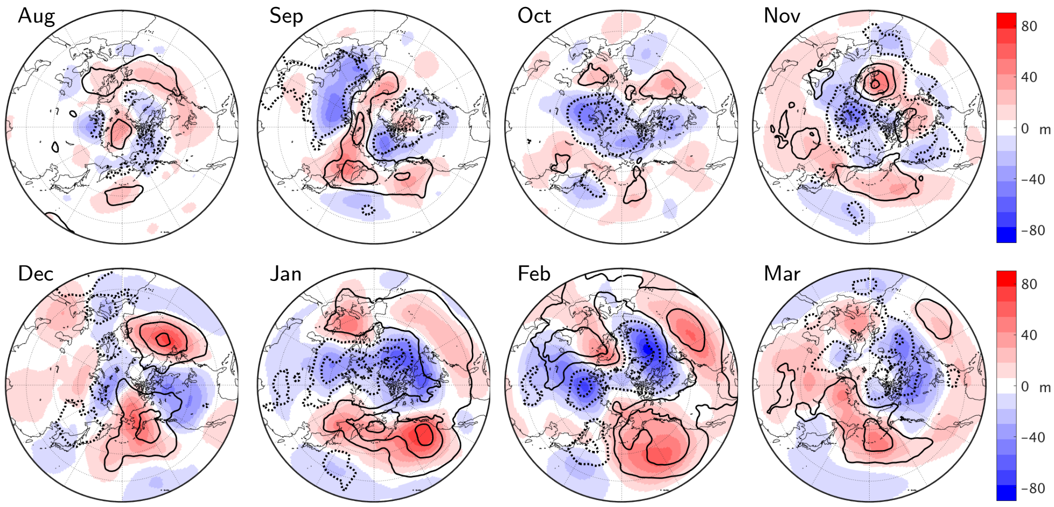

Figure 3.8: Observed monthly 500 mb geopotential height anomalies (shaded) and sea- level pressure anomalies (contours) for the Low regime. Contours begin at +/- 1 mb and have an interval of 2 mb. Positive (negative) SLP anomalies are shown by solid (dotted) contours. Statistical significance not shown.

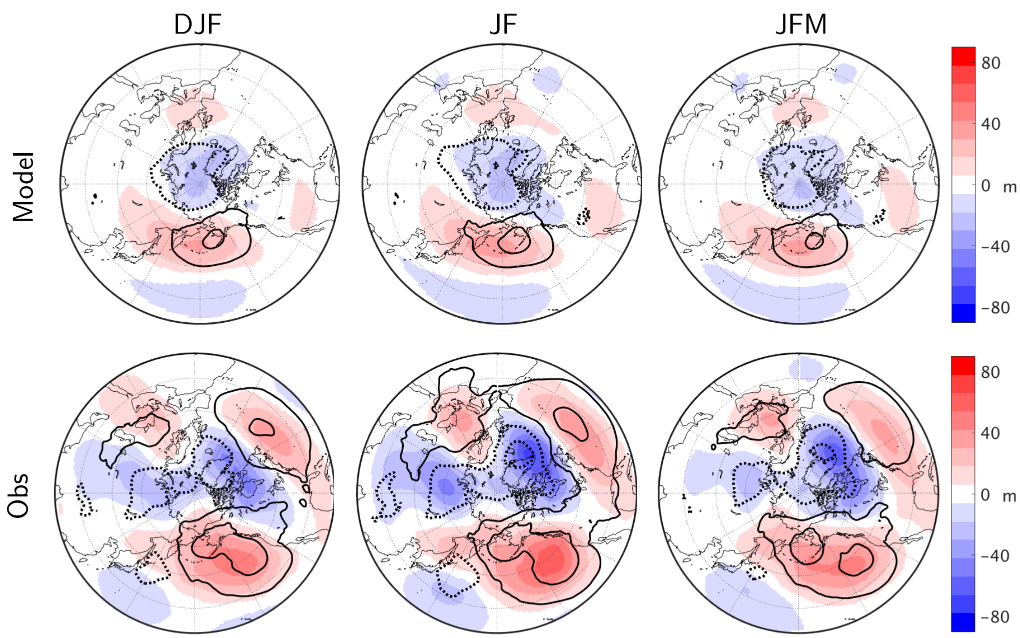

Figure 3.9: Z_{500} anomalies (shaded) and SLP anomalies (contours) averaged over multiple months for the Low regime. Contours begin at +/- 1 mb and have an interval of 2 mb. Positive (negative) SLP anomalies are shown by solid (dotted) contours.

Chapter 4
Conclusions

One goal of this study has been to gain further insight into the mechanisms responsible for creating anomalous February sea ice coverage in the Sea of Okshotsk (SOK) and the potential atmospheric response to these sea ice anomalies. To this end, we have investigated the conditions preceding and following anomalous February sea ice coverage in the SOK in both observations and simulations from the fully-coupled CESM-LE. Specifically, our other goal has been to compare the representation of these processes by CESM-LE with what has been observed in nature and documented in previous work. To achieve both of these goals, we have conducted composite analyses for both anomalously high and low sea ice years. Through this method, we have shown the monthly progression of conditions in the observations and of pre-winter conditions in the model, as well as the weekly progression of winter conditions in the model.

This study demonstrates how SOK sea ice variability in February is influenced by a multitude of factors at various time leads and how the atmosphere may respond to this variability. Extending back to the prior winter, SST anomalies exist in the SOK and western Bering Sea. These reach a temporary peak in magnitude during the summer prior to the SOK sea ice anomalies. THF anomalies then develop in autumn as low-level atmospheric temperature anomalies appear, affecting both the rate at which SSTs cool and the timing of initial sea ice formation. This thermodynamic mechanism also impacts early winter sea ice growth. Once sea ice growth has begun, its advection and the advancement of the sea ice edge are influenced by low-level winds generated by the anomalous SLP gradient between the Siberian high and the Aleutian low. Finally in February, THF anomalies in proximity to the average sea ice edge indicate abnormal heat transfer between the surface and the atmosphere. These THF anomalies may generate a dynamic response in the atmosphere above with a local SLP anomaly and with the excitation of a Rossby wave that extends across the North Pacific basin and terminates over North America.

Through comparison with observations, this study demonstrates the ability of CESM-LE to represent the causes of and response to anomalous SOK sea ice coverage with general accuracy. Results from this study support results from previous observational work regarding the mechanisms involved in setting up SOK sea ice anomalies (e.g., Ohshima et al., 2006; Nakanowatari et al., 2010; Sasaki et al., 2007). Our results are also consistent with previous work examining the impact of sea ice anomalies on atmospheric circulation (Alexander et al., 2004; Honda et al., 1999; Screen, 2017) and with the theoretical atmospheric response to a shallow, mid-latitude thermal forcing (Hoskins and Karoly, 1981; Vallis, 2017).

The atmospheric response to SOK sea ice has been shown to impact atmospheric circulation over North America (e.g., Screen, 2017), which could have motivated the use of SOK sea ice anomalies for seasonal weather prediction over North America. However, the small magnitude of the Z_{500} anomalies and the lack of significant θ_{850} anomalies over North America suggests that interannual SOK sea ice variability may not be useful for seasonal prediction may be limited. Yet this result does not preclude the potential for future, more extensive sea ice loss in this region to have notable impacts on atmospheric circulation over North America.

The results from this study raise further questions to be explored. For instance, the composite analysis employed here shows the average progression of conditions preceding and following anomalous sea ice coverage, not the progression of conditions that occur in any individual years. The relative importance of interseasonal SST anomalies, autumn thermodynamic preconditioning, and winter forcing in setting up anomalously low sea ice coverage in the SOK remains an open question. Furthermore, it is not clear from this analysis if each of these mechanisms are present in all anomalous sea ice years or if individual years are affected by a smaller number of mechanisms.

Additional questions outside the scope of this study are: What causes these persistent SST anomalies in the months prior to the February SOK anomalies? And why do they have a temporary peak in the late summer? One potential mechanism is incoming solar radiation anomalies at the surface due to abnormal cloud cover during the summer. Another possible factor is the transport of anomalous SSTs from another region in the North Pacific basin. If these interseasonal SST anomalies are present prior to most years of anomalous February SOK sea ice coverage, then understanding what causes them could add value to predicting winters of high or low sea ice.

Prediction of maximum sea ice extent in the SOK has already been undertaken with upwards of 70% of total variance explained (Sasaki et al., 2007; Nakanowatari et al., 2010). These predictive models incorporate variables such as 850 mb temperature, offshore component of the geostrophic wind, and SST in the vicinity of the SOK at lead times of one to three months. This study furthers our understanding of the processes responsible for generating interannual variability in sea ice coverage in the SOK, which could help to improve such predictive models. Extending these ideas to examine similar processes within the central Arctic could provide further understanding and predictability of interannual variability in Arctic sea ice coverage as that region eventually becomes seasonally ice-free.

Appendix | High Regime Figures

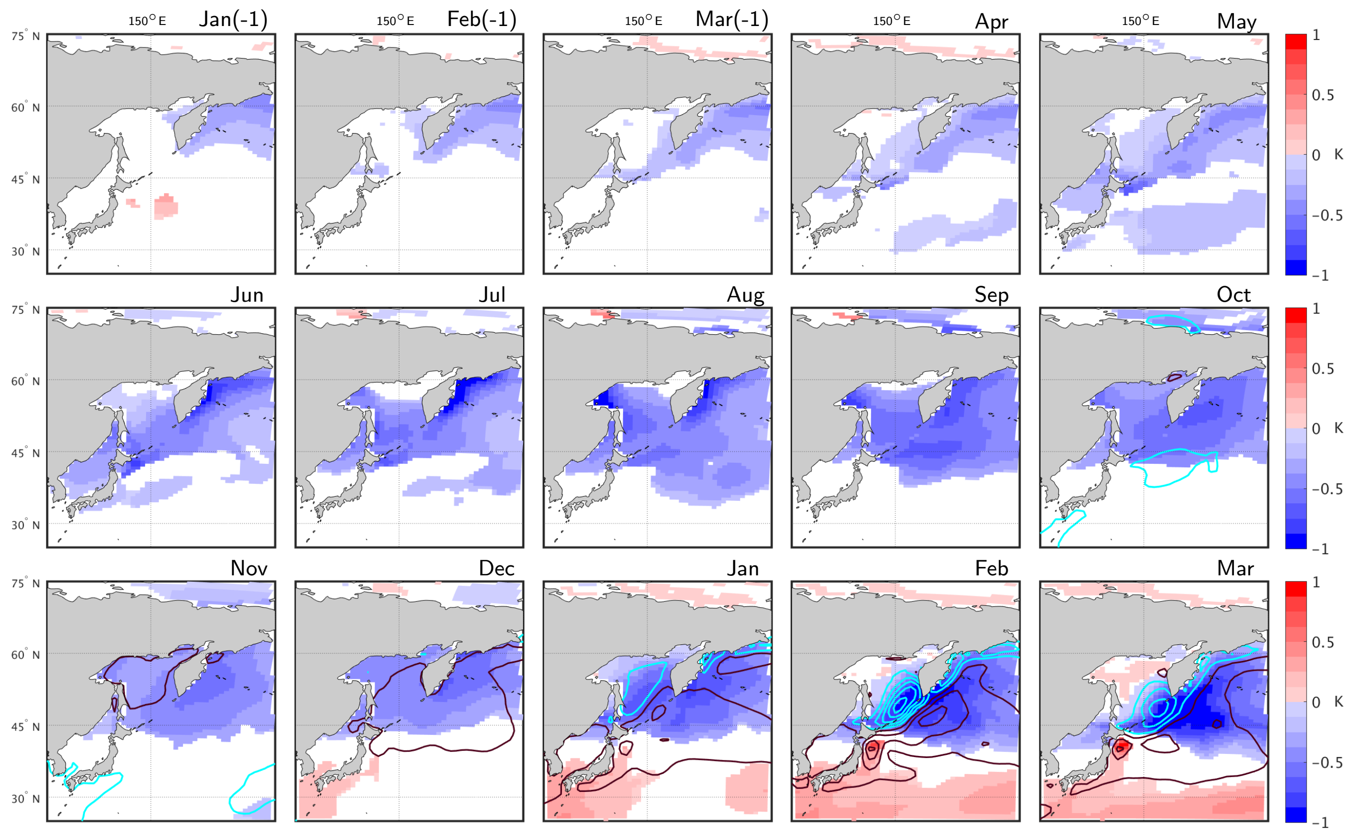

Figure A.1: Modeled monthly SST anomalies (shaded) and THF anomalies (contours) for the High regime. Contours begin at +/- 10 Wm^{-2} and have an interval of 10 Wm^{-2}. Positive (negative) THF anomalies are shown by maroon (cyan) contours and correspond to heat transfer out of (into) the surface. Only SST anomalies that are statistically significant at the α=0.05 level are shown.

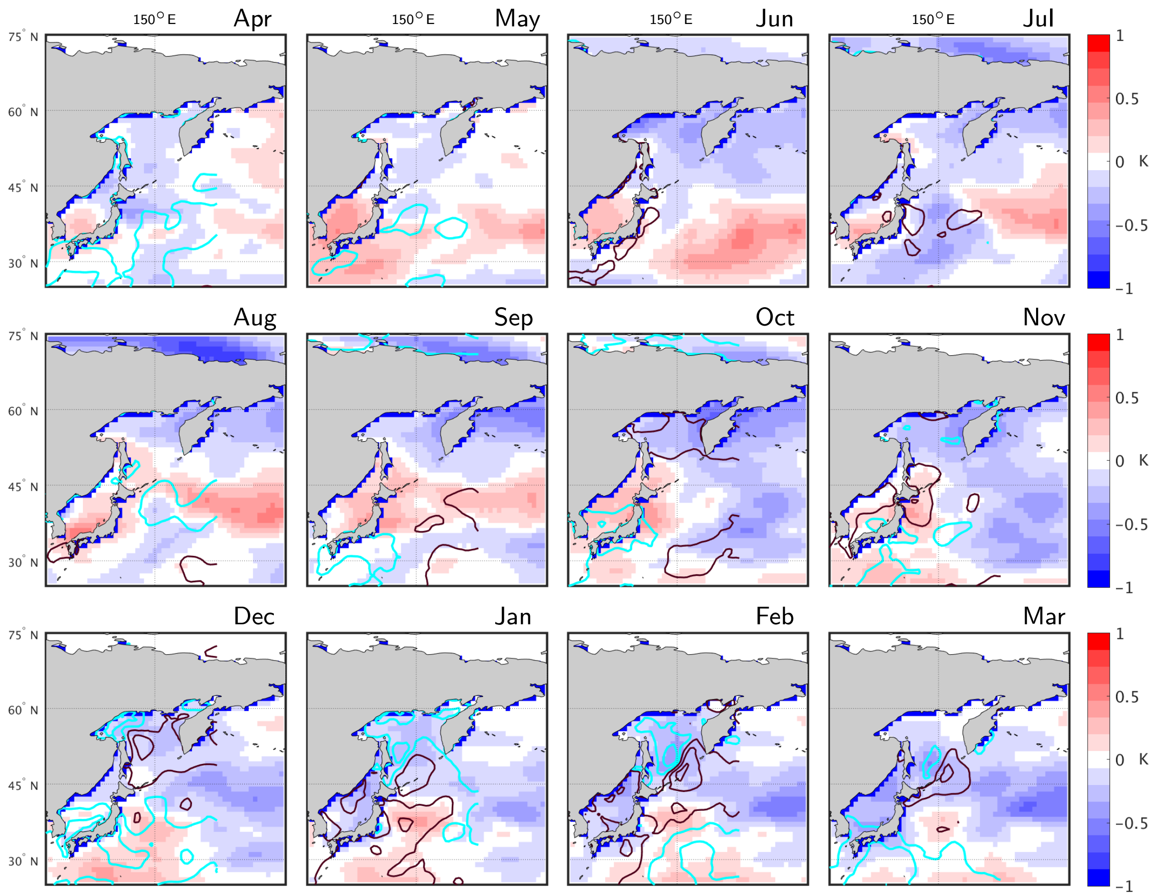

Figure A.2: Observed monthly SST anomalies (shaded) and THF anomalies (contours) for the High regime. Contours begin at +/- 10 Wm^{-2} and have an interval of 10 Wm^{-2}. Positive (negative) THF anomalies are shown by maroon (cyan) contours and correspond to heat transfer out of (into) the surface. Statistical significance not shown.

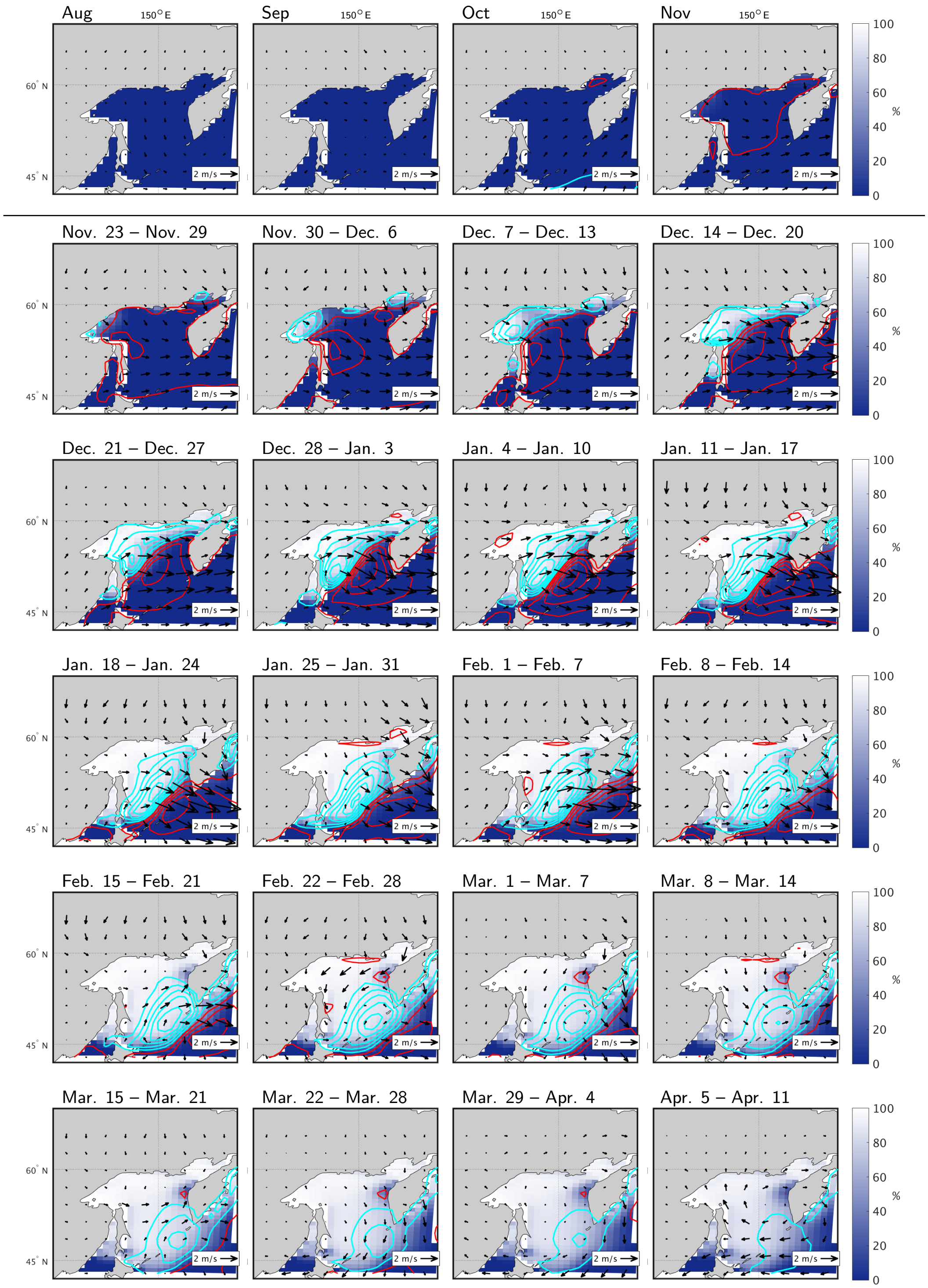

Figure A.3: Modeled total sea ice concentration (shaded) with THF anomalies (contours) and near-surface wind anomalies (arrows) for the High regime. Top row contains monthly-averaged values, while other rows contain weekly-averaged values. Contours begin at +/- 10 Wm^{-2} and have an interval of 20 Wm^{-2}. Positive (negative) THF anomalies are shown by red (cyan) contours.

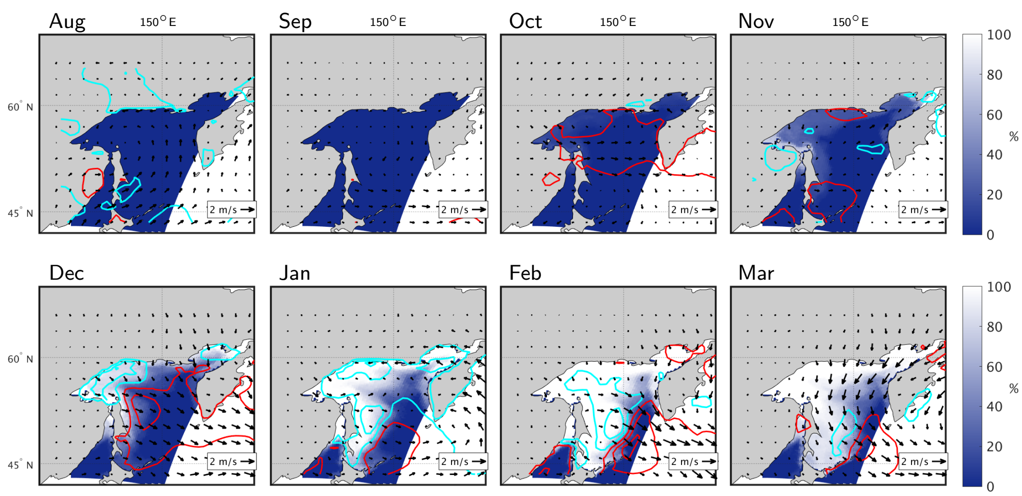

Figure A.4: Observed monthly total sea ice concentration (shaded) with THF anomalies (contours) and near-surface wind anomalies (arrows) for the High regime. Contours begin at +/- 10 Wm^{-2} and have an interval of 20 Wm^{-2}. Positive (negative) THF anomalies are shown by red (cyan) contours.

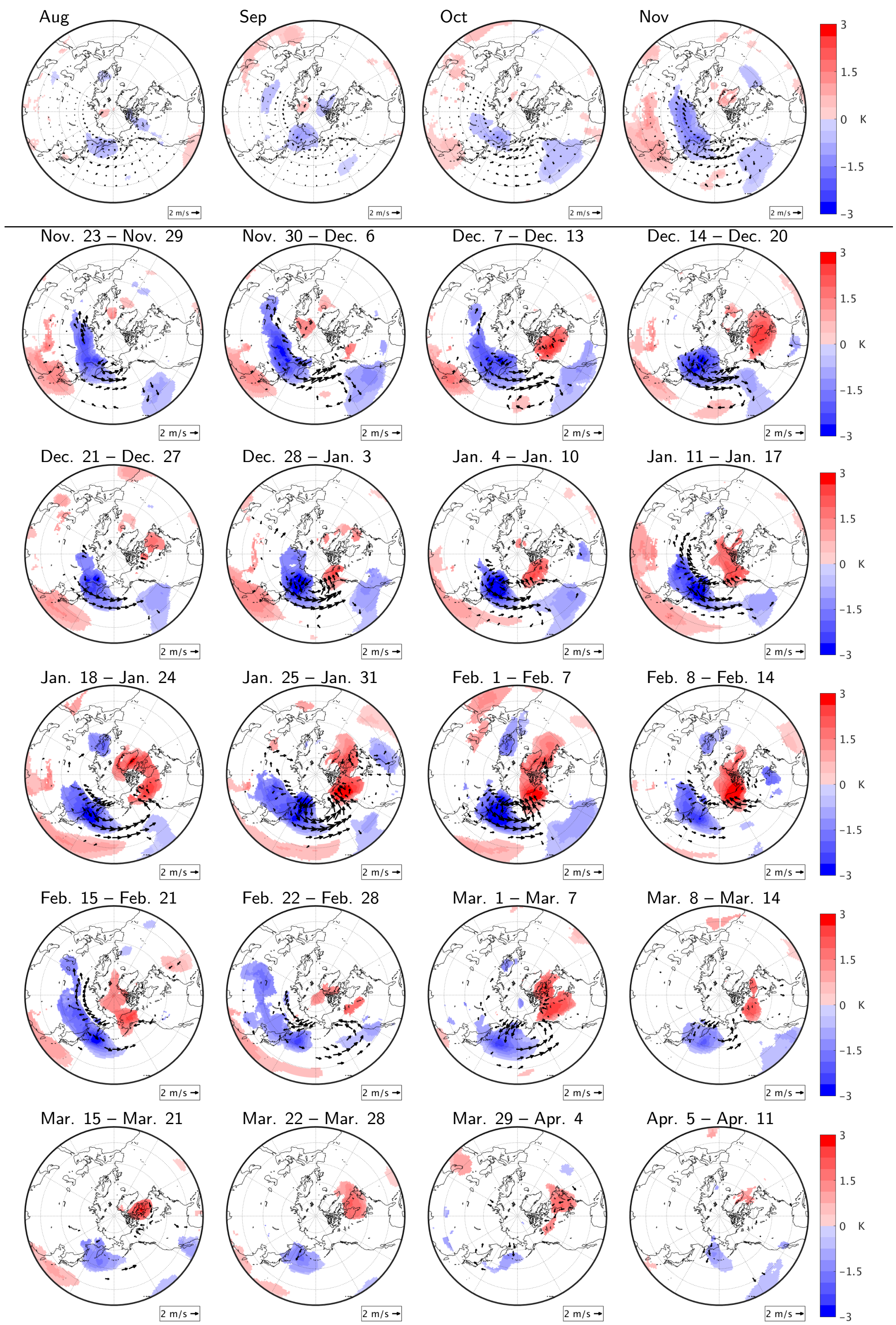

Figure A.5: Modeled 850 mb atmospheric anomalies: θ_{850} anomalies (shaded) and wind anomalies (arrows) for the High regime. Top row contains monthly-averaged values, while other rows contain weekly-averaged values. Plotted anomalies are statistically significant at the α=0.05 level.

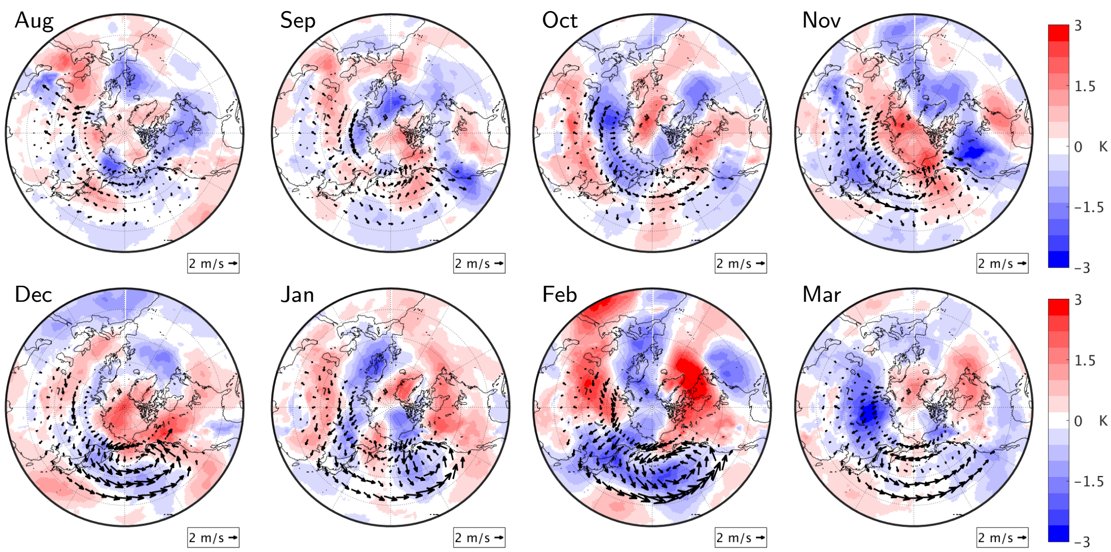

Figure A.6: Observed monthly 850 mb atmospheric anomalies: θ_{850} anomalies (shaded) and wind anomalies (arrows) for the High regime. Statistical significance not shown.

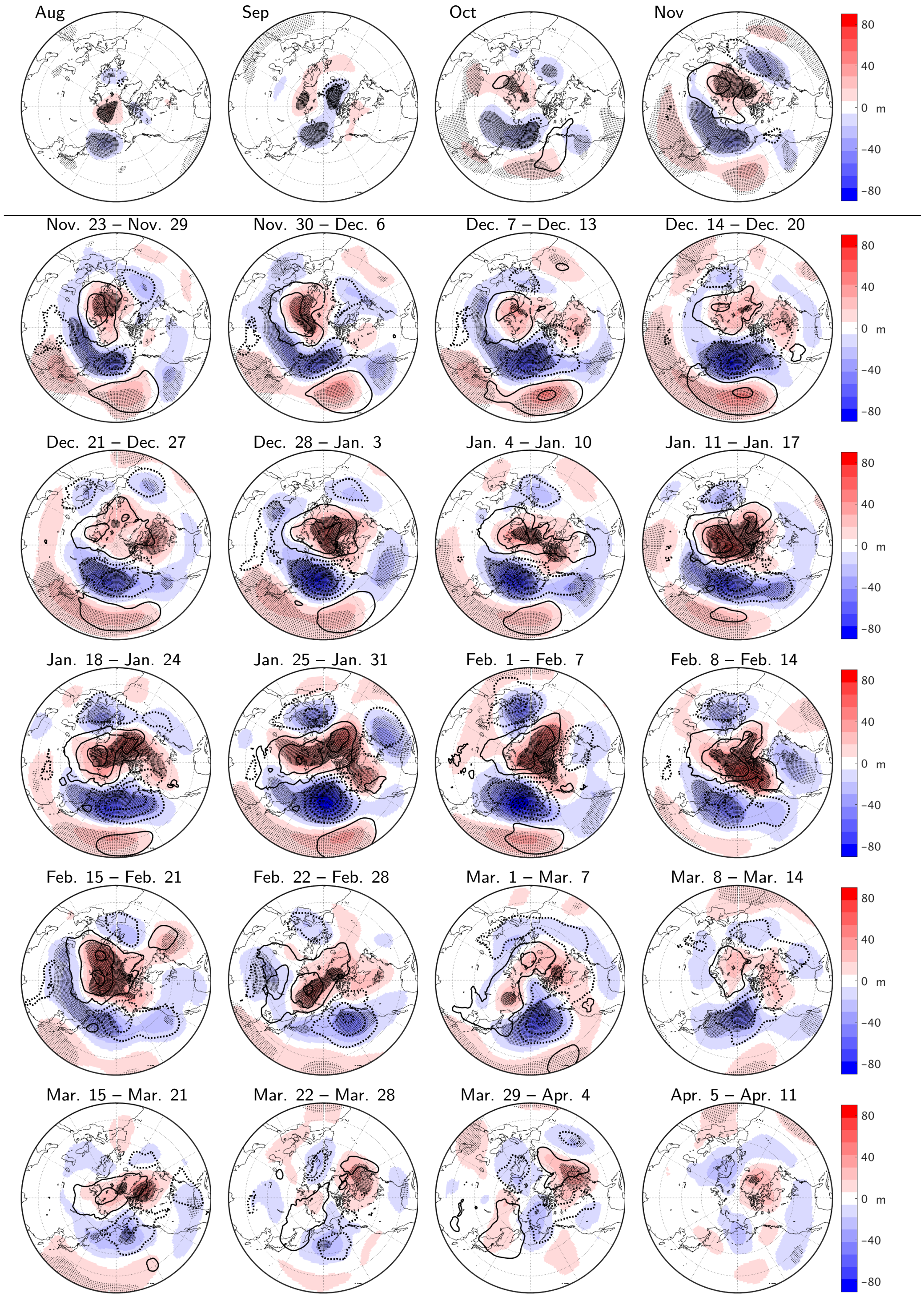

Figure A.7: Modeled 500 mb geopotential height anomalies (shaded) and sea- level pressure anomalies (contours) for the High regime. Top row contains monthly-averaged values, while other rows contain weekly-averaged values. Contours begin at +/- 1 mb and have an interval of 2 mb. Positive (negative) SLP anomalies are shown by solid (dotted) contours. Geopotential height anomalies are stippled if statistically significant at the α=0.05 level.

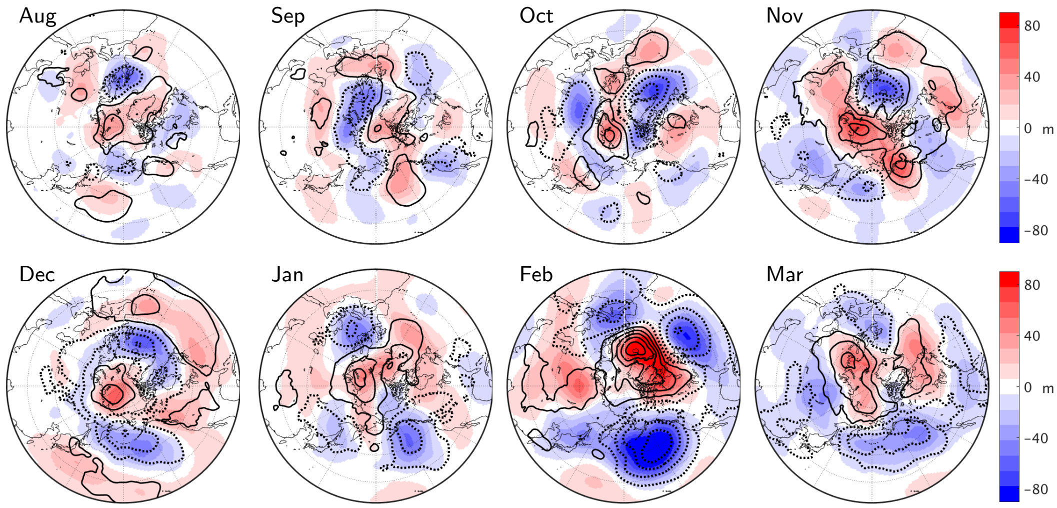

Figure A.8: Observed monthly 500 mb geopotential height anomalies (shaded) and sea- level pressure anomalies (shaded) for the High regime. Contours begin at +/- 1 mb and have an interval of 2 mb. Positive (negative) SLP anomalies are shown by solid (dotted) contours. Statistical significance not shown.

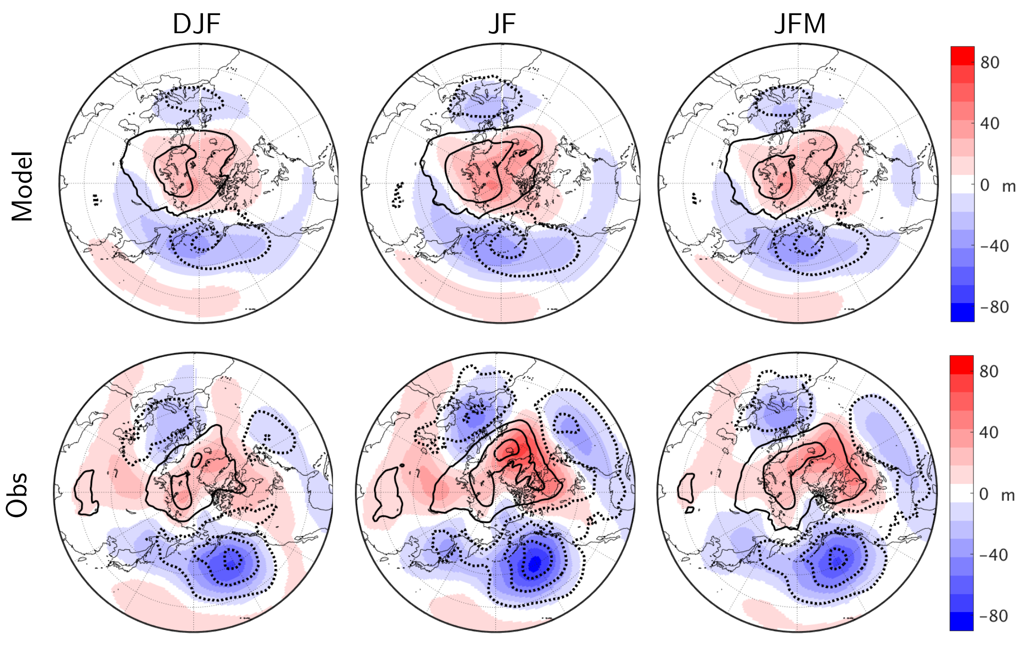

Figure A.9: Z_{500} anomalies (shaded) and SLP anomalies (contours) averaged over multiple months for the High regime. Contours begin at +/- 1 mb and have an interval of 2 mb. Positive (negative) SLP anomalies are shown by solid (dotted) contours.

Bibliography

Alexander, M. A., U. Bhatt, J. E. Walsh, M. S. Timlin, J. S. Miller, and J. D. Scott, 2004: The atmospheric response to realistic Arctic sea ice anomalies in an AOGCM during winter. *Journal of Climate*, **17**, 890–905.

Bitz, C. M., and W. H. Lipscomb, 1999: An energy-conserving thermodynamic model of sea ice. *Journal of Geophysical Research: Oceans*, **104 (C7)**, 15 669–15 677, doi:10.1029/1999jc900100.

Close, S., M. N. Houssais, and C. Herbaut, 2017: The Arctic winter sea ice quadrupole revisited. *Journal of Climate*, **30 (9)**, 3157–3167, doi:10.1175/JCLI-D-16-0506.1.

Dee, D. P., and Coauthors, 2011: The ERA-Interim reanalysis: Configuration and performance of the data assimilation system. *Quarterly Journal of the Royal Meteorological Society*, **137 (656)**, 553–597, doi:10.1002/qj.828.

Deser, C., M. A. Alexander, and M. S. Timlin, 2003: Understanding the persistence of sea surface temperature anomalies in midlatitudes. *Journal of Climate*, **16 (1)**, 57–72, doi:10.1175/1520-0442(2003)016<0057:UTPOSS>2.0.CO;2.

Fang, Z., and J. M. Wallace, 1994: Arctic sea ice variability on a timescale of weeks and its relation to atmospheric forcing. **7 (12)**, 1897–1914.

Gascard, J. C., K. Riemann-Campe, R. Gerdes, H. Schyberg, R. Randriamampianina, M. Karcher, J. Zhang, and M. Rafizadeh, 2017: Future sea ice conditions and weather forecasts in the Arctic: Implications for Arctic shipping. *Ambio*, **46**, 355–367, doi:10.1007/s13280-017-0951-5.

Honda, M. K., K. Yamazake, and K. Takeuchi, 1999: Dynamic and thermodynamic characteristics of atmospheric response to anomalous sea ice extent in the {Sea of Okhotsk}. *J. Climate*, **12**, 3347–3358, doi:10.1175/1520-0442(1999)012<3347:DATCOA>2.0.CO;2.

Hoskins, B. J., and D. J. Karoly, 1981: The Steady Linear Response of a Spherical Atmosphere to Thermal and Orographic Forcing. *Journal of the Atmospheric Sciences*, **38**, 1179–1196, doi:10.1175/1520-0469(1981)038<1179:TSLROA>2.0.CO;2.

Hunke, E. C., and J. K. Dukowicz, 2002: The Elastic-Viscous-Plastic Sea Ice Dynamics Model in General Orthogonal Curvilinear Coordinates on a Sphere – Incorporation of Metric Terms. *Monthly Weather Review*, **130 (7)**, 1848–1865, doi:10.1175/1520-0493(2002)130<1848:tevpsi>2.0.co;2.

Hunke, E. C., and W. H. Lipscomb, 2008: CICE: The Los Alamos Sea Ice Model, Documentation, and Software, Version 4.0. Tech. rep., Los Alamos National Laboratory Tech. Rep. LACC-06-012, 76 pp.

Hurrell, J. W., and Coauthors, 2013: The Community Earth System Model: A Framework for Collaborative Research. *Bulletin of the American Meteorological Society*, **94 (9)**, 1339–1360, doi:10.1175/bams-d-12-00121.1.

Ishii, M., A. Shouji, S. Sugimoto, and T. Matsumoto, 2005: Objective analyses of sea-surface temperature and marine meteorological variables for the 20th century using ICOADS and the Kobe Collection. *International Journal of Climatology*, **25 (7)**, 865–879, doi:10.1002/joc.1169.

Jahn, A., J. E. Kay, M. M. Holland, and D. M. Hall, 2016: How predictable is the timing of a summer ice-free Arctic? *Geophysical Research Letters*, **43**, 9113–9120, doi:10.1002/2016GL070067.

Kay, J. E., and Coauthors, 2015: The Community Earth System Model (CESM) Large Ensemble Project. *Bulletin of the American Meteorological Society*, **(August)**, 1333–1349, doi:10.1175/BAMS-D-13-00255.1.

Lawrence, D. M., and Coauthors, 2011: Parameterization improvements and functional and structural advances in Version 4 of the Community Land Model. *Journal of Advances in Modeling Earth Systems*, **3 (1)**, 1–27, doi:10.1029/2011ms00045.

Liu, J., Z. Zhang, R. M. Horton, C. Wang, and X. Ren, 2007: Variability of North Pacific sea ice and East Asia-North Pacific winter climate. *Journal of Climate*, **20 (10)**, 1991–2001, doi:10.1175/JCLI4105.1.

Meier, W., F. Fetterer, M. Savoie, S. Mallory, R. Duerr, and J. Stroeve, 2017: NOAA/NSIDC Climate Data Record of Passive Microwave Sea Ice Concentration, Version 3. [Dataset] [Feb. 1980 - Feb. 2000]. NSIDC: National Snow and Ice Data Center, [6 Jul 2018], doi:10.7265/N59P2ZTG.

Melia, N., K. Haines, E. Hawkins, and J. J. Day, 2017: Towards seasonal Arctic shipping route predictions. *Environmental Research Letters*, **12 (8)**, doi:10.1088/1748-9326/aa7a60.

Mesquita, M. D., K. I. Hodges, D. E. Atkinson, and J. Bader, 2011: Sea-ice anomalies in the Sea of Okhotsk and the relationship with storm tracks in the Northern Hemisphere during winter. *Tellus, Series A: Dynamic Meteorology and Oceanography*, doi:10.1111/j.1600-0870.2010.00483.x.

Nakanowatari, T., K. I. Ohshima, and S. Nagai, 2010: What determines the maximum sea ice extent in the Sea of Okhotsk? Importance of ocean thermal condition from the Pacific. *Journal of Geophysical Research: Oceans*, **115 (12)**, 1–10, doi:10.1029/2009JC006070.

Ogi, M., B. Taguchi, M. Honda, D. G. Barber, and S. Rysgaard, 2015: Summer-to-winter sea-ice linkage between the Arctic ocean and the Okhotsk sea through atmospheric circulation. *Journal of Climate*, **28 (12)**, 4971–4979, doi:10.1175/JCLI-D-14-00297.1.

Ohshima, K. I., S. Nihashi, E. Hashiya, and T. Watanabe, 2006: Interannual Variability of Sea Ice Area in the Sea of Okhotsk: Importance of Surface Heat Flux in Fall. *Journal of the Meteorological Society of Japan*, **84 (5)**, 907–919, doi:10.2151/jmsj.84.907, URL http://joi.jlc.jst.go.jp/JST.JSTAGE/jmsj/84.907?from=CrossRef.

Oleson, K. W., and Coauthors, 2010: Technical description of version 4.0 of the Community Land Model (CLM). NCAR Tech. Note NCAR/TN-478+STR, 257 pp.

Parkinson, C. L., 1990: The impact of the Siberian High and Aleutian Low on the sea-ice cover of the Sea of Okhotsk. *Annals of Glaciology*, **14**, 226–229, doi:10.3189/S0260305500008636.

Peings, Y., and G. Magnusdottir, 2013: Response of the wintertime northern hemisphere atmospheric circulation to current and projected arctic sea ice decline: A numerical study with CAM5. *Journal of Climate*, **27**, 244–264, doi:10.1175/JCLI-D-13-00272.1.

Peng, G., W. N. Meier, D. J. Scott, and M. H. Savoie, 2013: A long-term and reproducible passive microwave sea ice concentration data record for climate studies and monitoring. *Earth System Science Data*, **5**, doi:10.5194/essd-5-311-2013.

Rosenblum, E., and I. Eisenman, 2017: Sea ice trends in climate models only accurate in runs with biased global warming. *Journal of Climate*, **30 (16)**, 6265–6278, doi:10.1175/JCLI-D-16-0455.1.

Rothrock, D. A., 1975: The Energetics of the Plastic Deformation of Pack Ice by Ridging. *Journal of Geophysical Research*, **80 (33)**, 4514–4519.

Sasaki, Y. N., Y. Katagiri, S. Minobe, and I. G. Rigor, 2007: Autumn atmospheric preconditioning for interannual variability of wintertime sea-ice in the Okhotsk Sea. *Journal of Oceanography*, **63 (2)**, 255–265, doi:10.1007/s10872-007-0026-5.

Screen, J. A., 2017: Simulated atmospheric response to regional and pan-arctic sea ice loss. *Journal of Climate*, **30 (11)**, 3945–3962, doi:10.1175/JCLI-D-16-0197.1.

Smith, R., and Coauthors, 2010: The Parallel Ocean Program (POP) reference manual: Ocean component of the Community Climate System Model (CCSM) and Community Earth System Model (CESM). Tech. rep., Los Alamos National Laboratory Tech. Rep. LAUR-10-01853, 141 pp. URL http://www.cesm.ucar.edu/models/cesm1.0/pop2/doc/sci/POPRefManual.pdf.

Sun, L., C. Deser, and R. A. Tomas, 2015: Mechanisms of stratospheric and tropospheric circulation response to projected Arctic sea ice loss. *Journal of Climate*, **28 (19)**, 7824–7845, doi:10.1175/JCLI-D-15-0169.1.

Thorndike, A. S., D. A. Rothrock, G. A. Maykut, and R. Colony, 1975: The thickness distribution of sea ice. *Journal of Geophysical Research*, **80 (33)**, 4501–4513, doi:10.1029/jc080i033p04501.

Ukita, J., M. Honda, H. Nakamura, Y. Tachibana, D. J. Cavalieri, C. L. Parkinson, H. Koide, and K. Yamamoto, 2007: Northern Hemisphere sea ice variability: Lag structure and its implications. *Tellus, Series A: Dynamic Meteorology and Oceanography*, **59 (2)**, 261–272, doi:10.1111/j.1600-0870.2006.00223.x.

Vallis, G. K., 2017: *Atmospheric and Oceanic Fluid Dynamics: Fundamentals and Large-Scale Circulation*, 585–626. 2nd ed., Cambridge University Press, Cambridge, doi:10.1017/9781107588417.017.

Yamamoto, K., Y. Tachibana, M. Honda, and J. Ukita, 2006: Intra-seasonal relationship between the Northern Hemisphere sea ice variability and the North Atlantic Oscillation. *Geophysical Research Letters*, **33 (14)**, 2–6, doi:10.1029/2006GL026286.